

Measuring supermassive black holes via reverberation mapping in the UV

Shai Kaspi¹ 

Received: 31 December 2017 / Accepted: 18 March 2018 / Published online: 29 March 2018
© Springer Science+Business Media B.V., part of Springer Nature 2018

Abstract Over the past three decades the reverberation mapping technique was used to measure the central regions of Active Galactic Nuclei (AGN), their size, velocity field, and the mass of the black hole in the center. This technique was used mainly in the optical with several studies in the UV. Reverberation mapping in the UV adds essential information to the AGN studies. This paper reviews these recent studies done in the UV, presents results from the recent HST campaign toward NGC 5548, and discuss two projects of reverberation mapping of UV emission lines in high-luminosity quasars. The advantages of reverberation mapping in the UV will be discussed as well as the needs from new UV missions in order to be able to advance UV reverberation mapping campaigns.

Keywords Quasars · Black holes · Reverberation mapping · Broad line region · AGN

1 Introduction

Active Galactic Nuclei (AGNs) are centers of galaxies which show strong activity which manifest itself with strong luminosity from the center of the galaxy (of order 10 to 1000 times more than normal galaxies), and with variation of that luminosity over different timescales. The spectrum of AGNs is composed of non-thermal continuum with multiple broad

(FWHM of order of a few thousands km s^{-1}) and narrow (FWHM of order of a few hundreds km s^{-1}) emission lines. The current general paradigm for an AGN is a supermassive black hole (SMBH) at the center of the galaxy which accrete matter via an accretion disk that is responsible for the continuum radiation. Around this accretion disk there are clouds of photoionized material which are called the Broad Line Region (BLR) and are responsible for the broad lines emission. A molecular torus is around the BLR and much further away are clouds of low ionization material which is the Narrow Line Region (NLR) that is responsible for the narrow lines emission. Another important component for the above picture is the jet which is probably perpendicular to the accretion disk (e.g., Urry and Padovani 1995, Fig. 1).

Phenomenologically AGNs are divided into different groups depending on different characteristics. One of the main division is for AGNs which show both broad and narrow emission lines and are called type 1 AGNs, and AGNs which show only narrow emission line with no broad emission lines—these are called type 2 AGNs. In the context of the above model, type 1 are objects in which their torus is at face-on angles to the observer and thus both the BLR and NLR are seen, and type 2 AGNs are objects which their torus is at edge-on angles to the observer and thus only the NLR is seen and the BLR is obscured by the torus. Another division is to AGNs which have low luminosity and are called Seyfert galaxies (and are usually at low redshifts) and to AGNs with high luminosity which are called quasars (and are usually at high redshifts). The border line between Seyferts and Quasars is at bolometric luminosity of about $10^{44} \text{ erg s}^{-1}$.

In order to study the AGN phenomenon relations between different characteristics of AGNs were studied over the years. One of the main relation that was studied is the relation between the distance from the SMBH to the BLR,

This article belongs to the Topical Collection: UV Surveys, the Needs and the Means. Guest Editors: Ana I. Gómez de Castro, Noah Brosch.

✉ S. Kaspi
shai@wise.tau.ac.il

¹ School of Physics and Astronomy and Wise Observatory, Raymond and Beverly Sackler Faculty of Exact Sciences, Tel-Aviv University, Tel-Aviv 69978, Israel

the luminosity of the AGN, and the mass of the SMBH in its center. These are all measurable parameters and therefore they are fundamental characteristics of AGNs and tight relations between them are expected. In the following sections I will focus on these relations based on observations from the UV. In Sect. 2 the reverberation mapping technique is described. In Sect. 3 current BLR-Size–Luminosity–Mass relations are described, and in Sect. 4 reverberation mapping in the UV and its implications are described.

2 Reverberation mapping

2.1 Measurement of the BLR size

Reverberation mapping is a technique to measure the distance between the central SMBH and the BLR, in which for simplicity we will refer to this distance in the following as the “BLR size”. In fact this technique gives only a weighted mean of that distance since the BLR is stratified and the BLR size that is measured is only an approximation for the distance between the central SMBH and the BLR. Reverberation mapping is based on the fact that the BLR is responding to variation in the continuum flux. The continuum flux of AGNs is known to vary on different time scales, probably because the matter which accretes into the SMBH is clumpy in nature, causing different amount of material to accrete at different times and causing variations in the luminosity of the AGN. When these variations in the continuum luminosity arrive to the BLR they cause variations in the flux of the emission lines via the process of photoionization of the BLR. These variations in the emission-lines flux are following the variations of the continuum flux due to the distance between the SMBH and its accretion disk to the BLR, R (Fig. 1). The time lag, Δt , between the variations in the continuum flux and the variations in the emission-line flux is connected with R via the simple relation with the speed of light velocity, c : $R = c\Delta t$. The idea of the response of emission lines flux in a photoionized nebula to variations of the emission from the illuminating central source was first suggested by Bahcall et al. (1972) and first measured by Cherepashchuk and Lyutyi (1973).

The entire BLR does not respond at the same time. A cloud at a distance R from the central source and angle θ to the line of sight (see Fig. 1) will appear to respond after a time: $t = R/c(1 - \cos\theta)$. If the BLR’s clouds are ordered in a certain geometry around the SMBH then the response of the emission line will be an integration of the responses from all the BLR. The response of complicated geometries, such as thick spherical shells and thin disks, to a short continuum flash, can be calculated by integrating the above response over distance and radius. For example, a thick shell BLR will respond to a continuum flash from the central source as

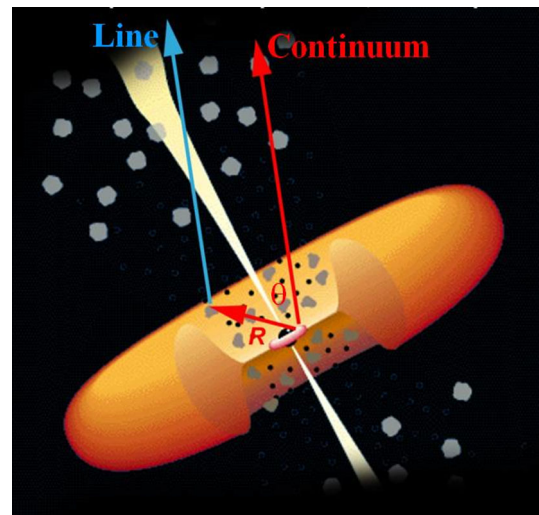
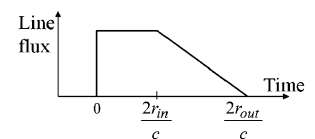


Fig. 1 Reverberation mapping schematics based on the AGN model of Urry and Padovani (1995)

Fig. 2 Response of a thick shell BLR with inner radius of r_{in} and outer radius r_{out} to a flash in the continuum flux



described in Fig. 2. The continuum flash is at time $t = 0$ and the line flux response continues up to $t = 2r_{out}/c$, where r_{out} is the outer radius of the thick shell. Also, the response of all those geometries to a complicated change in the continuum can be obtained by integrating over the δ -functions assembling it. From those simple examples it can be seen that for each geometry and each change in continuum flux, there is a unique response of the emission lines.

Blandford and McKee (1982) coined the term “reverberation mapping” and put it into mathematical formulation. They refer to the technique as finding the “transfer function”. The transfer function describes the response of an emission-line to a δ -function continuum outburst. The actual continuum behavior in AGNs is complex, and as a result the emission line response is the convolution of the continuum variation and the transfer function. In general, the relationship between the continuum light-curve $C(t)$ and the emission-line light-curve $L(v, t)$ can be described by

$$L(v, t) = \int_{-\infty}^{\infty} \Psi(v, \tau) C(t - \tau) d\tau, \quad (1)$$

which is known as the “transfer equation”. The aim is usually to use the observables $C(t)$ and $L(v, t)$ to solve this integral equation for $\Psi(v, \tau)$, the transfer function, and thus infer the geometry and kinematics of the BLR. In the original formulation of Blandford and McKee (1982), the transfer function is obtained by Fourier methods using the con-

olution theorem

$$\tilde{\Psi}(\omega) = \frac{\tilde{L}(\omega)}{\tilde{C}(\omega)}, \tag{2}$$

where $\tilde{L}(\omega)$ is the Fourier transform of $L(t)$, etc., and then transforming $\tilde{\Psi}(\omega)$ back to the time domain. Several theoretical works have studied transfer functions for BLRs with different geometries and velocity fields (e.g., Pérez et al. 1992, and references therein). However, in practice a stable and unique solution for $\Psi(v, \tau)$ requires a large amount of high-quality data, and this is the main limitation of reverberation mapping. Since high quality spectra of faint objects are not easy to obtain, we will focus on the somewhat simpler problem of solving for the *one-dimensional transfer function* $\Psi(\tau)$, which gives the response of the entire emission line integrated over line-of-sight velocity, i.e.,

$$L(t) = \int_{-\infty}^{\infty} \Psi(\tau)C(t - \tau)d\tau. \tag{3}$$

In real situations, solution by Fourier transforms does not work very well since the data are not regularly sampled, and a very large number of points are required. Thus, this one dimension reverberation mapping is simplified into simple cross correlation of the line and continuum light curves.

Cross-correlation techniques, that were used in astronomy for accurate radial velocity measurements, were first introduced into BLR reverberation experiments by Gaskell and Sparke (1986). Actual light curves are sets of numbers that need to be cross-correlated in order to measure the time lag. Thus it can be expressed as a sum of two unnormalized data sets

$$CCF(\tau) = \frac{1}{N\sigma_C\sigma_L} \sum_t C(t)L(t + \tau), \tag{4}$$

where N is the number of points, σ_C and σ_L are the rms of the light-curves, and the two light-curves have zero means. τ is an arbitrary temporal shift between the two data sets. The lag is the value of τ which maximizes the correlation coefficient between the two series. To carry out this calculation, the data points need to be evenly spaced, and for a given $C(t)$, $L(t + \tau)$ needs to be measured. Also, the time base of the light-curves needs to be large and the object needs to vary during this time in order to get meaningful results. Those conditions are usually hard to achieved. Bad weather, and period during which the objects cannot be observed, introduce gaps in the data and the object variations are, of course, unpredictable.

One method to overcome some of those difficulties is the interpolated cross-correlation function (ICCF) method of Gaskell and Sparke (1986) and Gaskell and Peterson (1987) as implemented by White and Peterson (1994). In

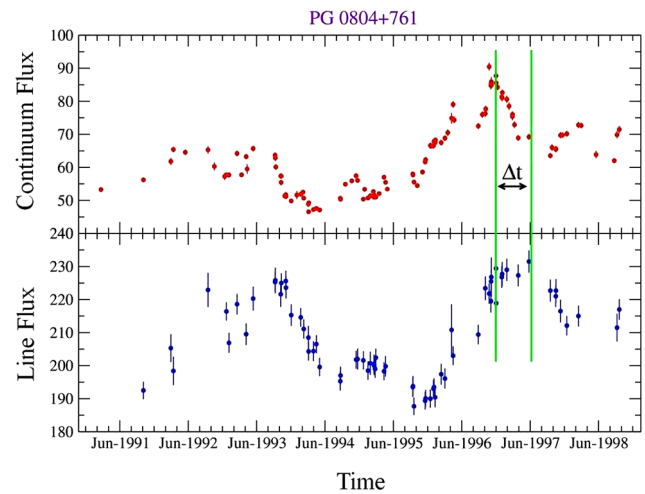


Fig. 3 Light curves for PG 0804+761. Top panel: continuum flux at the wavelength of 5100 Å in the rest frame in units of 10^{-16} ergs cm^{-2} s^{-1} Å $^{-1}$. Bottom panel: the H α light curve in units of 10^{-14} ergs cm^{-2} s^{-1} . The time lag, Δt in clearly seen between the two light curves. Data are from Kaspi et al. (2000)

this method, the CCF is calculated twice for the two observed light curves $C(t_i)$ and $L(t_i)$: once by pairing the observed $C(t_i)$ with the interpolated value $L(t_i - \tau)$, and once by pairing the observed $L(t_i)$ with the interpolated value $C(t_i - \tau)$. The final CCF is taken to be the average of these two CCFs. An optional feature is to extrapolate one light curve at a constant level to avoid discarding data. Another method is the z -transformed discrete correlation function (ZDCF: Alexander 1997) which is an improvement of the Discrete Correlation Function (DCF) method suggested by Edelson and Krolik (1988). The ZDCF applies Fisher’s z transformation to the correlation coefficients, and uses equal population bins instead of the equal time bins that are used in the DCF. To estimate the uncertainties on the time lags determined by of the above two methods the model-independent Monte Carlo method called Flux Randomization/Random Subset Selection (FR/RSS) of Peterson et al. (1998) is commonly used.

As an example, Fig. 3 shows the continuum and H β emission line light curves as measured for PG 0804+761 over 7.5 years. The time lag between the two light curves is clearly seen. Figure 4 shows the CCF of these two light curves with a peak at 187^{+29}_{-37} days.

2.2 Mass determination

In order to calculate the mass of the SMBH we use the assumption that the BLR clouds are moving in virialized motion around it (see Sect. 4 below for a justification of that assumption). Thus, we can use the equality between the gravitational force in which the SMBH pulls the BLR clouds and the centrifugal force that drives away the BLR clouds from

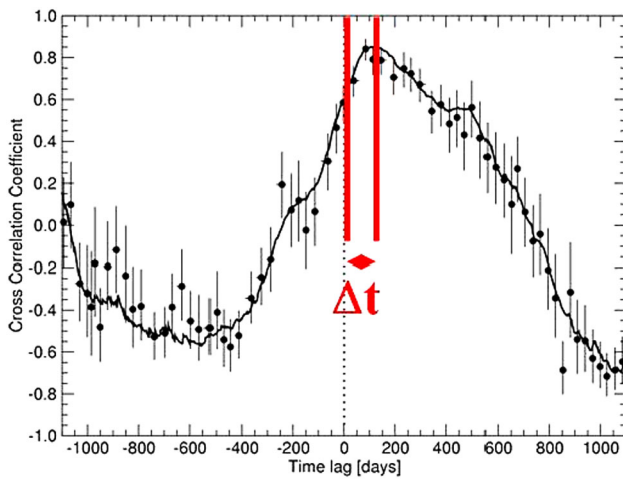


Fig. 4 CCF for the light curves which are shown in Fig. 3. Solid line is the ICCF and points with uncertainties are from the ZDCF. Both methods are consistent with each other

the SMBH due to their motion in Keplerian orbits. From such an equality one drives that the mass of the SMBH is:

$$M_{BH} = f \frac{V^2 R}{G} \tag{5}$$

where G is the gravitational constant, V is the velocity of the clouds, and f is a constant of order of unity which holds in it the geometry of the BLR clouds, their orientation, and the relation between the measured R and V to their actual values.

As mentioned in Sect. 2.1, once the time lag is measured, the distance R can be calculated by multiplying the time lag by the speed of light. However, this is only a measure of the BLR size since the BLR can have a complex shape and the time lag is an average over the response of the entire BLR.

V is estimated from the width of the broad emission line, since that broadening is due to the motion of the clouds around the SMBH. There are two main methods to estimate V , one is to measure the FWHM of the line, and the second one is to use the second moment of the line profile to define the variance, or mean square dispersion, of the line in which its square root gives the line dispersion, σ_{line} , which then used as V (see discussion in Peterson et al. 2004). Whichever method is used, this has some effect on the value of f which is used in (5).

3 Current BLR-Size–Luminosity–Mass Relations

During the past three decades almost 100 AGNs were studied using the reverberation mapping technique and got sufficient data to determine the distance of their BLR from their SMBH. The vast majority of these objects were studied in their $H\beta$ line and the continuum at a restframe

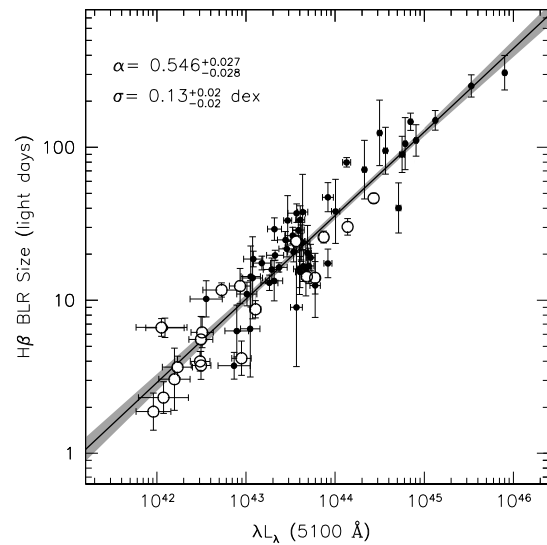


Fig. 5 $H\beta$ BLR size versus the luminosity at 5100 Å. Adopted from Bentz et al. (2013)

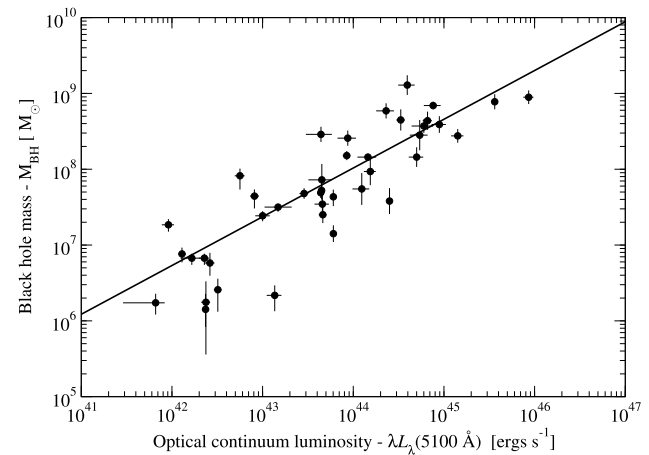


Fig. 6 SMBH mass versus the luminosity at 5100 Å. Adopted from Kaspi (2012)

wavelength of 5100 Å, because this is the easiest line and continuum spectrum to be observed from ground optical telescopes (e.g., Wandel et al. 1999; Kaspi et al. 2000; Bentz et al. 2013). In Fig. 5 we show the relation between R and L (at 5100 Å) as obtained by Bentz et al. (2013). These data yield the following relation:

$$R_{H\beta} \propto [\lambda L_{\lambda}(5100 \text{ \AA})]^{(0.546 \pm 0.027)}. \tag{6}$$

Such a relation was obtained over the years also for luminosities at other wavelengths and similar relations were calculated (e.g., Kaspi et al. 2005).

In Fig. 6 we show the mass luminosity relation as obtained by Kaspi (2012).

Once the above BLR-Size–Luminosity–Mass Relations were determined for these AGNs and the relations were

measured and calibrated, they are now used to determine the mass of the SMBH in practically any type 1 AGN. This is done by using the “single epoch mass determination” method. In this method only one spectrum of the AGN is observed and calibrated. From this spectrum the AGN luminosity is determined and using the R – L relation (e.g., Fig. 5) the value of R is estimated. The velocity of the BLR clouds is estimated by measuring V from the single spectrum that was obtained and thus using (5) the mass of the SMBH is determined from this single spectrum. An alternative way is to use the relation of M_{BH} and L (e.g., Fig. 6) to determine the mass of the SMBH directly from L which is measured from the single epoch spectrum, although this method is considered less accurate since this relation is a result of calculations of M_{BH} using the measured R and V as explained in Sect. 2.2, with the uncertainties that are entering into this calculation as explained there.

Using the single epoch mass determination the mass of thousands of SMBH in large samples of AGNs can be determined and then can be used for many statistical studies such as the cosmological evolution of AGNs, mass function, accretion history, and more.

4 Reverberation mapping in the UV and implications

4.1 Importance of reverberation mapping in the UV

First reverberation mapping project in the UV was done by Clavel et al. (1991) with the International UV Explorer (IUE) on the AGN NGC 5548. The UV spectroscopic monitoring was done over 8 months during 1989 and 60 epochs were obtained. From these spectra they extracted light curves of a few UV emission lines as well as light curves of the continuum at different wavelengths. Cross correlation of the line with continuum light curves resulted with the time delays for the different lines as presented in Table 1. In parallel to these IAU observations also an optical ground based monitoring took place to monitor the $H\beta$ line variation, and this resulted with a time delay of about 10–25 days (Netzer et al. 1990). One of the main results of the above campaign is that high ionization ions reside at smaller distances from the SMBH than low ionization ions. Thus, the BLR is stratified with high ionization ions closer to the central radiation source.

Following the above UV observations with IUE on NGC 5548 in 1989 a few other monitoring campaigns toward type 1 AGNs were carried with IUE: NGC 3783 in 1992 (Reichert et al. 1994), NGC 5548 in 1993 (Korista et al. 1995), 3C 390.3 in 1995 (O’Brien et al. 1998), NGC 7469 in 1996 (Wanders et al. 1997). Also few HST monitoring observations were carried: NGC 5548 in 1993 (Korista et al.

Table 1 NGC 5548 time lags

Emission lines	Time lag [days]
HeII λ 1640 & NV λ 1240	4–10
L α λ 1216 & CIV λ 1549	8–16
SiIV λ 14202 & CIII λ 1909	12–34
MgII λ 2798	34–72
H β	10–25

Note: UV data are from Clavel et al. (1991)

H β time lag is from (Netzer et al. 1990)

1995), NGC 4395 in 2004 (Peterson et al. 2005), NGC 5548 in 2014 (De Rosa et al. 2015).

Using the data of the three objects: NGC 7469, NGC 5548, and 3C 390.3, Peterson and Wandel (2000) showed that the FWHM of lines with different ionization levels are consistent with Keplerian motions. This was shown from the relation between V (found from the FWHM) and the time lag that was found to be consistent with the following relation:

$$V \propto \tau^{-1/2} \propto R^{-1/2} \quad (7)$$

see their Fig. 1. This is consistent with one of the fundamental assumption of reverberation mapping as presented in Sect. 2.2 above and confirms the assumption at the base of this technique which enables the determination of the mass of the SMBH. We note that this was done only for a few objects and it is important to verify this for more objects. The UV observations are *essential* since only in them information from different species of ions, both low- and high-ionization, can be measured with large enough separation in ionization between them to be able to determine the different time lags and different velocities (V), and thus to get the relation described in (7).

Recently, the most state of the art UV reverberation mapping campaign was carried out using HST toward one of the most studied AGNs. The program, called “AGN Space Telescope and Optical Reverberation Mapping” (STORM), was a multi-wavelength reverberation mapping monitoring program to study the Seyfert 1 galaxy NGC 5548, during 2014 January to August. NGC 5548 was observed in the Far-UV with HST once per day for 171 orbits. Simultaneously with the HST observations also NIR-MIR photometry monitoring was carried out using ground based telescopes and the Spitzer IR space observatory. Optical ground based spectroscopy and photometry daily monitoring was carried out as well. X-Ray monitoring was carried out with Chandra and SWIFT space observatories, and Optical-NUV photometry was carried out with SWIFT three times per day.

This campaign yielded the most spectacular data set ever obtained in a reverberation mapping campaign. NGC 5548

showed strong continuum and line flux variations and thus time lags in the UV (relative to the 1367 Å continuum) were determined in unprecedented accuracy: Ly α $7.73^{+0.57}_{-0.76}$ days, SiIV $7.22^{+1.06}_{-1.33}$ days, CIV $9.24^{+1.04}_{-1.04}$ days, and for HeII $3.87^{+0.71}_{-0.58}$ days (De Rosa et al. 2015). Comparing these time lags with the width of each of the lines De Rosa et al. found that the shortest time lags were found for the ions which show the highest velocity. This again confirms the stratification of the BLR in which higher ionization lines reside in the inner parts of the BLR closer to the SMBH and that it is consistent with Keplerian motions.

One of the most interesting result form the above recent campaign toward NGC 5548 is described in Goad et al. (2016). During the campaign the UV emission lines responded to the continuum during the first ~ 75 days, but then for about 50–60 days the emission lines decoupled from the continuum variations and did not follow with the same variability (see their Fig. 1). Only during the last ~ 40 days of the campaign the emission lines returned to follow the continuum variations. This is the first time that such a behavior of the continuum is unambiguously identified in an AGN reverberation mapping campaign. The largest discrepancy between the emission line and the continuum during this period of no response occurred for the high ionization, collisionally excited lines CIV, SiIV, and HeII, while the anomaly in Ly α was substantially smaller. Goad et al. (2016) suggested two scenarios to explain this behavior of the BLR, either there was a temporary obscuration of the BLR (e.g., by material ejected from the disk), or there was a temporary change in the ionizing continuum (e.g., by a changed SED).

The detection of this event is stressing again the importance of reverberation mapping in the UV and its high impact for our understanding AGNs.

4.2 Broadening the luminosity range to low luminosities

Until 2004 only four AGNs were monitored in the UV as mentioned in the previous paragraph. All of them were scattered around UV luminosity of $\lambda L_{\lambda}(1350 \text{ \AA}) \sim 10^{44} \text{ ergs s}^{-1}$ as can be seen in Fig. 7. Thus, a relation between the BLR distance from the SMBH derived from the UV emission lines and the UV luminosity could not be determined. In order to broaden the luminosity range Peterson et al. (2005) carried out a reverberation mapping campaign toward NGC 4395 which is the least luminous type 1 AGN. The spectroscopic observations were done with HST and included two visits of five orbits each. A time lag of order 1 hour was measured for the CIV from both visits. Since NGC 4395 is four orders of magnitude lower in luminosity than the previously studied AGNs in the UV, this new measurement enabled for the first time to determine the $R-L$

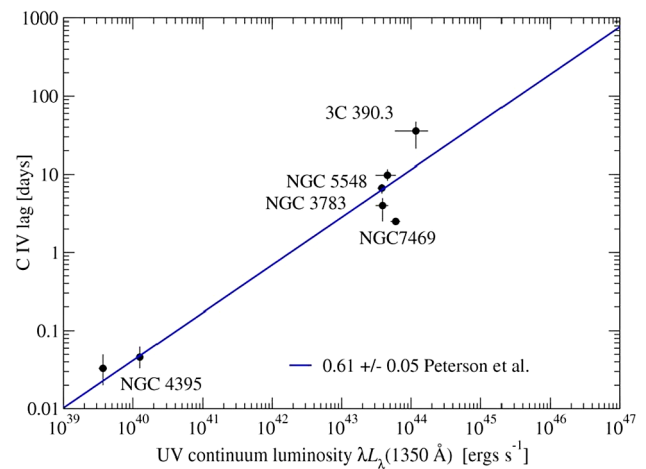


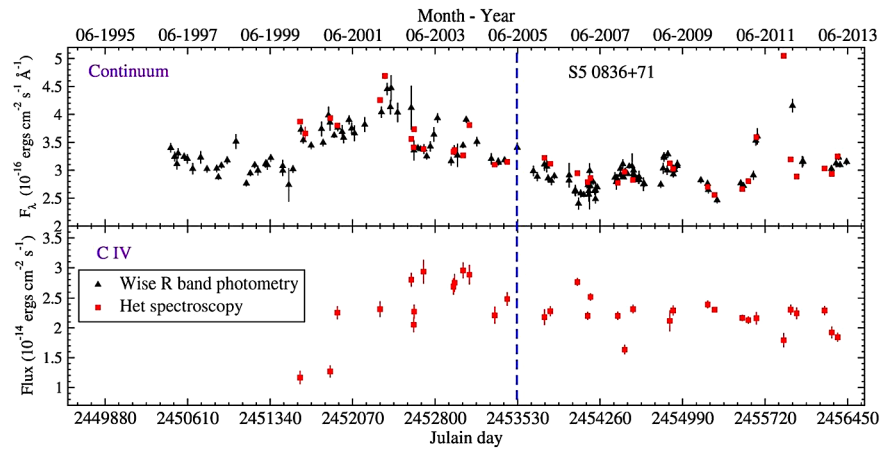
Fig. 7 CIV time lag as a function of the UV luminosity for objects with reverberation mapping observations in the UV

relation in the UV, as seen in Fig. 7. However, there are only few objects studied in the UV and more UV reverberation mapping campaigns are needed in order to better study this parameter range and elevate it to the number of objects with reverberation mapping in the optical range (Fig. 5).

4.3 Broadening the luminosity range to high luminosities

The AGN phenomenon ranges over eight orders of magnitude in UV luminosity. Though, as seen in Fig. 7 no significant results from reverberation mapping of UV lines were obtained for the high-luminosity AGNs in the range $10^{44} < \lambda L_{\lambda}(1350 \text{ \AA}) < 10^{47} \text{ ergs s}^{-1}$. High-luminosity AGNs are also the ones with high redshift. Thus, the UV lines are redshifted into the optical range and monitoring of the UV emission lines and the UV continuum can be carried out by ground based optical telescopes. However, only a few attempts of RM for higher luminosity AGNs were carried out thus far and with very limited success (e.g., Welsh et al. 2000; Trevese et al. 2014). Such attempts are difficult to carry out due to several reasons: higher luminosity AGNs have larger BLR distances from the central source and longer variability time scales. Thus, monitoring periods of order a decade are needed for such projects and observations cadence needs to be of order a month. Telescope time allocation committees are usually reluctant to commit telescope time for such long periods. Also, the variability amplitude of high-luminosity AGNs are smaller than low-luminosity AGNs and the BLR size is larger, thus causing the line response to be smeared making line variations harder to detect. Yet another difficulty is that the light curves are stretched by the cosmic time dilation, further extending the monitoring period, thus the response of the BLR gas is harder to detect.

Fig. 8 Light curves for S5 0836+71. Red squares are points measured from the spectroscopic data and black triangles are points measured from the photometric data. The top panel is the continuum light curve (spectroscopic points measured on the red side of the C IV line). The bottom panel is line light curves for C IV. Data up to the blue vertical dashed line were published in Kaspi et al. (2007)



In order to fill the above missing luminosity range and to overcome the above problems we initiated in 1995 a photometric monitoring of 11 quasars. After a few years we started spectroscopic monitoring of six of these quasars at the Hobby–Eberly Telescope (HET; Ramsey et al. 1998). The six object were the only ones from our sample of 11 quasars that were accessible to the HET since it is limited and cannot observe objects at declinations higher than 72 degrees. The six objects are in the luminosity range of $10^{46} < \lambda L_{\lambda}(5100 \text{ \AA}) < 10^{47.5} \text{ erg s}^{-1}$ and redshift range of $2 \lesssim z \lesssim 3.4$. Their observed magnitudes are $V \lesssim 18$, and they have high declination in order to maximize the monitoring period during the year from northern hemisphere telescopes. That monitoring campaign and some results from the first 5 years were presented by Kaspi et al. (2007).

The sample was observed photometrically monthly in the *B* and *R* bands for about 8 months each year. Spectroscopy of the sample was done about three times a year, evenly spaced over the period of observability which is about 6 months. To obtain cross calibration between the different spectroscopic epochs we included in the slit a comparison star which was aligned with the quasar (e.g., Kaspi et al. 2000).

In Fig. 8 we show the light curves of S5 0836+71 as an example from our sample. All the eleven objects we monitored photometrically show continuum variations of about 20% to 60% (measured relative to the minimum flux). Line variations were detected only in a few of the lines we monitored. The reason for not detecting line variations can be because of their low variations that were not detected in our data, or that the continuum variation that pass the large BLR are smeared and no variations in the lines could be detected.

The CCF for the light curves from Fig. 8 is shown in Fig. 9. We find significant time lags for C IV in 3 of our 6 objects, for the C III] line in one of the objects, and a possible time lag of Ly α in one of the objects. The full results

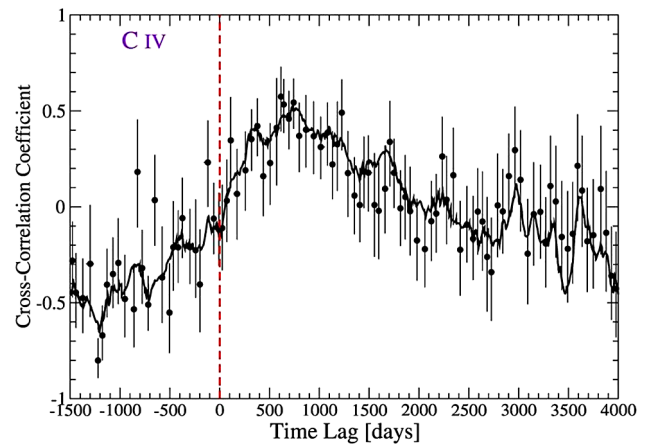


Fig. 9 CCFs for the light curves shown in Fig. 8. The ICCF method is shown as a solid line and the ZDCF method is shown as filled circles with uncertainties. Time lags are given in the observed frame. The measured time lag is 730^{+289}_{-188} days in the observed frame

from that project will be published in Kaspi et al. (2018, in preparation).

Another reverberation mapping campaign which we have been conducting in the past decade is of a sample of 17 AGNs from the Calan–Tololo and SDSS catalogs. These objects all have UV luminosity of $\lambda L_{\lambda}(1350 \text{ \AA}) < 10^{47.5} \text{ erg s}^{-1}$ and a redshift range of $2.3 < z < 3.4$. Photometric observations were carried out at the 0.9 m CTIO telescope every ~ 2 months since 2005 and upon detection of 15% variability, spectroscopy follow was triggered with the 2.5 m DuPont telescope at LCO. Results from a decade monitoring were submitted for publication (Lira et al. 2018, submitted). For several of these 17 AGNs we are able to measure statistically significant time lags for the Ly α (3 objects), SiIV, C IV (5 objects), and C III] lines, while for one source we obtain a MgII line time lag. The results of this study show that the Ly α and C IV emitting regions are found at similar distances from the central source, which is about four times closer

than the $H\beta$ distance. For the MgII and CIII] the emitting regions are ~ 4 to 5 times further away.

5 Summary

In the past three decades the BLR size of almost 100 AGNs was measured with the $H\beta$ emission line and a tight correlation with the luminosity was established with a slope of ~ 0.5 . Using the width of the emission line the mass of the SMBH was directly determined for these objects.

UV reverberation mapping established there is a radial ionization stratification in the BLR and that the BLR clouds motion are virial and primarily orbital. To determine the BLR size and measure the masses of high-luminosity high-redshift quasars we have measured their UV lines which are redshifted to the optical. In order to scale the relation of the Radius–Luminosity relation of the UV lines (seen in the optical) with the relation measured for low luminosity AGNs (Seyferts), mainly with the $H\beta$ line, we have to monitor many of them in the UV.

From the examples shown in Sect. 4 the reverberation mapping campaigns in the UV can be split into main two categories. One category is studies to determine the time lags of the UV lines in numerous objects. To achieve this we need a moderate resolution spectrograph that will be able to dedicate substantial amount of time for reverberation mapping of AGNs. This can be an IUE kind of spectrograph, or a more modern version like the FOS on HST. This spectrograph should have resolution of a few \AA , and aperture to include in it a point source as all AGNs to be in reverberation mapping projects are point sources. The second category is studies to monitor in depth the UV lines and their profiles with reverberation mapping studies (e.g., same as the recent NGC 5548 campaign). In such studies there is a need for a high resolution spectrograph like the STIS or COS on board HST with resolution of order 0.1 \AA , and aperture to include in it a point source. Such studies will yield not only the time lag but also the dynamics and geometry of the BLR.

Since the lines monitored in the UV are at longer wavelength than $Ly\alpha$ the spectrograph for reverberation mapping needs to have wavelength range starting from 1000 \AA and up to the optical wavelength so to be able to study also lines in the UV that are redshifted.

Reverberation mapping in the UV allow us to obtain further information about AGNs which cannot be gathered in other wavelengths and thus these UV observations are vital for the future research of AGNs.

References

- Alexander, T.: In: Maoz, D., Sternberg, A., Leibowitz, E.M. (eds.) *Astronomical Time Series*, p. 163 (1997). https://doi.org/10.1007/978-94-015-8941-3_14
- Bahcall, J.N., Kozlovsky, B.-Z., Salpeter, E.E.: *Astrophys. J.* **171**, 467 (1972). <https://doi.org/10.1086/151300>
- Bentz, M.C., Denney, K.D., Grier, C.J., et al.: *Astrophys. J.* **767**, 149 (2013). <https://doi.org/10.1088/0004-637X/767/2/149>
- Blandford, R.D., McKee, C.F.: *Astrophys. J.* **255**, 419 (1982). <https://doi.org/10.1086/159843>
- Cherepashchuk, A.M., Lyutyi, V.M.: *Astrophys. Lett.* **13**, 165 (1973)
- Clavel, J., Reichert, G.A., Alloin, D., et al.: *Astrophys. J.* **366**, 64 (1991). <https://doi.org/10.1086/169540>
- De Rosa, G., Peterson, B.M., Ely, J., et al.: *Astrophys. J.* **806**, 128 (2015). <https://doi.org/10.1088/0004-637X/806/1/128>
- Edelson, R.A., Krolik, J.H.: *Astrophys. J.* **333**, 646 (1988). <https://doi.org/10.1086/166773>
- Gaskell, C.M., Peterson, B.M.: *Astrophys. J. Suppl. Ser.* **65**, 1 (1987). <https://doi.org/10.1086/191216>
- Gaskell, C.M., Sparke, L.S.: *Astrophys. J.* **305**, 175 (1986). <https://doi.org/10.1086/164238>
- Goad, M.R., Korista, K.T., De Rosa, G., et al.: *Astrophys. J.* **824**, 11 (2016). <https://doi.org/10.3847/0004-637X/824/1/11>
- Kaspi, S.: In: Sulentic, J.W., Marziani, P., D’Onofrio, M. (eds.) *Fifty Years of Quasars: From Early Observations and Ideas to Future Research*, vol. 386, p. 298 (2012). https://doi.org/10.1007/978-3-642-27564-7_9
- Kaspi, S., Smith, P.S., Netzer, H., Maoz, D., Jannuzi, B.T., Giveon, U.: *Astrophys. J.* **533**, 631 (2000). <https://doi.org/10.1086/308704>
- Kaspi, S., Maoz, D., Netzer, H., et al.: *Astrophys. J.* **629**, 61 (2005). <https://doi.org/10.1086/431275>
- Kaspi, S., Brandt, W.N., Maoz, D., Netzer, H., Schneider, D.P., Shemmer, O.: *Astrophys. J.* **659**, 997 (2007). <https://doi.org/10.1086/512094>
- Kaspi, S., Brandt, W.N., Maoz, D., Netzer, H., Schneider, D.P., Shemmer, O.: *Astrophys. J.* (2018, in preparation)
- Korista, K.T., Alloin, D., Barr, P., et al.: *Astrophys. J. Suppl. Ser.* **97**, 285 (1995). <https://doi.org/10.1086/192144>
- Lira, P., Botti, I., Kaspi, S., et al.: *Astrophys. J.* (2018, submitted)
- Netzer, H., Maoz, D., Laor, A., et al.: *Astrophys. J.* **353**, 108 (1990). <https://doi.org/10.1086/168594>
- O’Brien, P.T., Dietrich, M., Leighly, K., et al.: *Astrophys. J.* **509**, 163 (1998). <https://doi.org/10.1086/306464>
- Pérez, E., Robinson, A., de La Fuente, L.: *Mon. Not. R. Astron. Soc.* **256**, 103 (1992). <https://doi.org/10.1093/mnras/256.1.103>
- Peterson, B.M., Wandel, A.: *Astrophys. J. Lett.* **540**, L13 (2000). <https://doi.org/10.1086/312862>
- Peterson, B.M., Bentz, M.C., Desroches, L.-B., et al.: *Astrophys. J.* **632**, 799 (2005). <https://doi.org/10.1086/444494>
- Peterson, B.M., Ferrarese, L., Gilbert, K.M., et al.: *Astrophys. J.* **613**, 682 (2004). <https://doi.org/10.1086/423269>
- Peterson, B.M., Wanders, I., Horne, K., et al.: *Publ. Astron. Soc. Pac.* **110**, 660 (1998). <https://doi.org/10.1086/316177>
- Ramsey, L.W., Adams, M.T., Barnes, T.G., Booth, J.A., Cornell, M.E., Fowler, J.R., et al.: In: Stepp, L.M. (ed.) *Proc. SPIE Advanced Technology Optical/IR Telescopes VI*, vol. 3352, p. 34 (1998). <https://doi.org/10.1117/12.319287>
- Reichert, G.A., Rodriguez-Pascual, P.M., Alloin, D., et al.: *Astrophys. J.* **425**, 582 (1994). <https://doi.org/10.1086/174007>
- Trevese, D., Perna, M., Vagnetti, F., Saturni, F.G., Dadina, M.: *Astrophys. J.* **795**, 164 (2014). <https://doi.org/10.1088/0004-637X/795/2/164>
- Urry, C.M., Padovani, P.: *Publ. Astron. Soc. Pac.* **107**, 803 (1995). <https://doi.org/10.1086/133630>
- Wandel, A., Peterson, B.M., Malkan, M.A.: *Astrophys. J.* **526**, 579 (1999). <https://doi.org/10.1086/308017>
- Wanders, I., Peterson, B.M., Alloin, D., et al.: *Astrophys. J. Suppl. Ser.* **113**, 69 (1997). <https://doi.org/10.1086/313054>
- Welsh, W., Robinson, E.L., Hill, G., Shields, G., Wills, B., Brandt, N., et al.: *Bull. Am. Astron. Soc.* **32**, 1458 (2000)
- White, R.J., Peterson, B.M.: *Publ. Astron. Soc. Pac.* **106**, 879 (1994). <https://doi.org/10.1086/133456>